Full Paper

Applied Organometallic Chemistry

Received: 14 September 2009 Revised: 17 January 2010 Accepted: 18 January 2010 Published online in Wiley Interscience: 4 March 2010

(www.interscience.com) DOI 10.1002/aoc.1632

Purification–chemical structure–electrical property relationship in gold nanoparticle liquids

Robert I. MacCuspie[a,b], Andrea M. Elsen[a], Steve J. Diamanti[a], Steve T. Patton[a,c], Igor Altfeder[a], J. David Jacobs[a], Andrey A. Voevodin[a] and Richard A. Vaia[a]*

Macroscopic assemblies of nanoparticles with fluid like characteristics, i.e. nanoparticle liquids (NPLs), are a new class of materials that exhibit unique properties compared with dispersions of nanoparticles in a molecularly distinct matrix phase. By focusing on reaction ratios, techniques to maximize concentration of reactants and quantification of chemical content during washing steps, a high degree of control over the purity of NPLs was maintained while allowing for easy scalability in batch sizes and synthesis throughput. A range of tertiary amines and quaternary ammoniums were used to successfully synthesize Au NPLs from a range of Au nanoparticles with nominal diameters from 6 to 20 nm and initially stabilized with either citrate or dodecanethiol. Stable Au NPLs after purification exhibited a sub-equivalence ratio of canopy to ligand molecules within the corona. This small canopy density most likely arose from the incommensurate areal density of anionic charge within the ligand shell relative to the larger size of the cationic canopy molecule, resulting in a population of cation–anion pairs too weakly bound to be retained in the initial assembly of the canopy post-purification. Finally, increasing either the volume fraction or molecular weight of the canopy was found to increase exponentially the electrical resistance of the bulk NPLs. Removal of excess canopy molecules created a conductive Au NPL that improved hot-current switching durability by at least two orders of magnitude beyond prior reports. Published in 2010 by John Wiley & Sons, Ltd.

Supporting information may be found in the online version of this article.

Keywords: nanoparticle liquids; gold nanoparticles; RF-MEMS switch; XPS

Introduction

Nanoparticle assemblies exhibiting liquid-like characteristics are a new class of materials with diverse applications ranging from self-healing materials to compliant electrodes. Referred to as nanoparticle liquids (NPLs),[1,2] solvent-free nanofluids,[3] solventless nanosalts[4] or self-lubricating ball bearings,[5] these single component nanocomposites exhibit viscoelastic or Newtonian character in a solvent-free state, at temperatures around or greater than ambient. In addition to the potential for a greater inorganic volume fraction due to the absence of an organic matrix phase, the liquid character affords novel self-assembly and green processing methodologies with zero volatile organic content.[6] Adding electrical conductivity to these characteristics is critical for many soft device concepts, including compliant electrodes, reconfigurable contacts and novel electro-rheological fluids within micro-fluidic devices.[7,8] Numerous examples of two-phase nanocomposite concepts that consist of conducting nanoparticles, such as metallic nanoparticles or carbon nanotubes, dispersed in polymers, have been previously reported for these applications;[9,10] however the antithetical relationships between processing, dispersion and inorganic fraction fundamentally limit formulation attempts to improve the overall property suite. In contrast, recent reports of NPLs have shown that sub-monolayer coatings of gold and platinum NPLs on electrical contacts increase the durability of low and high current switching in model RF-MEMS devices by over three orders of magnitude.[1,2,11,12]

One of the first reported observations of viscous behavior of a nanoparticle assembly showed physical slumping of a pellet of gold nanoparticles (AuNPs) at elevated temperatures.[13,14] This behavior was attributed to local melting of the alkyl passivation,[13] which subsequently disrupted the face-centered-cubic organization of the nanoparticle superstructure. Recently, the alkane passivation has been replaced with an equimolar electrostatic motif (i.e. an ionic liquid) in which one of the ionic species is covalently bound to the nanoparticle surface. This replacement has been explicitly demonstrated with metal[2,14,15] and metal oxide[16–19] nanoparticles. Conceptually, assemblies of functionalized nanoparticles should exhibit viscous and visco-elastic characteristics within a given region of temperature–pressure

* *Correspondence to: Richard A. Vaia, AFRL/RXBN, 2941 Hobson Way, WPAFB, OH 45433, USA. E-mail: richard.vaia@wpafb.af.mil*

a *Air Force Research Laboratory, Wright Patterson AFB, OH 45433, USA*

b *National Institute of Standards and Technology, Gaithersburg, MD, 20899-8520, USA*

c *University of Dayton Research Institute, Dayton, Ohio, USA*

space; however, the relationship between the organic surface functionalization, nanoparticle size and the collective motion of the nanoparticles is only now being tentatively explored.[20]

To continue to improve the combination of electrical conduction and viscous flow found in metallic NPLs, a fundamental understanding of the relationship between these physical characteristics and the nanoparticle size, passivation chemistry and corona dynamics is required. Within this paper the entire functionalization on the nanoparticle will be referred to as the *corona*, which is composed of a covalently-bound ionic *ligand shell* and its electrostatically bound *canopy*. Scalable synthesis routes that afford purification and quantification of bound and free organic moieties are paramount, as electrical properties of bulk NPL assemblies are very sensitive to inter-particle separation distances as well as the composition and quantity of the interspersed material. Herein, we discuss the impact of composition and purity of intermediate products on the creation of the electrostatic corona surrounding the AuNP. The generality and robustness of the resulting synthetic scheme is demonstrated for AuNPs derived from various fabrication methods. Finally, the relationship of d.c. conductivity, purity and corona composition is examined for Au NPLs ranging in nominal diameter from 6 to 20 nm, and is used to demonstrate that improved control over composition enabled even greater improvement in RF-MEMS switch device performance.

Experimental†

Reagents

The following reagents were purchased from Sigma-Aldrich (St Louis, MO, USA) with the highest purity available and were used as received without further purification. Abbreviations and molecular weights (MW) are listed afterwards in parentheses and brackets, respectively: methyltrialkyl (C8–C10) ammonium chloride (trade name Adogen 464) (AD) [MW = 464 unified atomic mass units (u)]; tris(2-ethylhexyl)amine (T2EH) [MW = 353 u]; triisooctylamine (TI8) [MW = 353 u]; triisopentylamine (TI5) [MW = 227 u]; tripentylamine (T5) [MW = 227 u]; trihexylamine (T6) [MW = 269 u]; trioctylamine (T8) [MW = 353 u]; 1,3-bis(2,6-diisopropylphenyl)imidazolium chloride [MW = 425 u]; 1,3-diisopropylimidazolium chloride [MW = 188 u]; 3-mercaptopropanesulfonate (MPS); sodium citrate; gold (III) chloride; sodium borohydride; chlorotriphenylphosphine gold (I); *t*-butylamineborane complex; dodecanethiol; and toluene. MaSurf FS-1620 (FS) and Maquat SL-15 (SL15) were purchased from Mason Chemical Company (Arlington Heights, IL, USA) and used as received. Arquad T-50 (AT), and Ethoquad T/13-27 W (ET), were purchased from AkzoNobel Surface Chemistry (Chicago, IL, USA), and used as received.

Synthesis Procedures

The general synthesis process is outlined in Scheme 1. Key aspects with regard to quantifying product composition are discussed in the next section. The complete stochiometric and electrostatically balanced organic functionalization assembly on the nanoparticle surface constitutes the already mentioned *corona*, which is composed of a covalently-bound ionic *ligand shell* and its electrostatically bound *canopy*. An important difference in this proposed synthesis process and previous work[3] is the use of AuNPs with a small anionic ligand shell and bulky cationic canopy, compared with previously used bulky cationic ligand shells and bulky anionic canopies,[17,18] and similar to recent reports of small anionic ligand shells and bulky cationic canopies surrounding SiO_2 nanoparticles.[21] Nevertheless, the purification and characterization procedures and conclusions are generally applicable irrespective of the electrostatic motif.

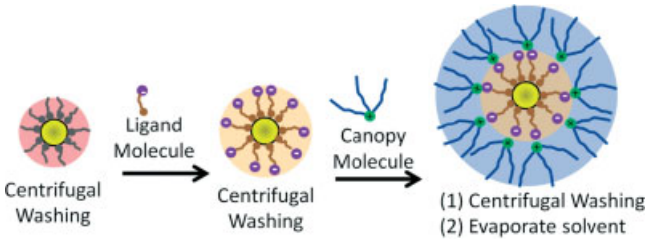

Scheme 1. Illustration of nanoparticle reaction scheme.

As an example, consider the fabrication of a T5 NPL. Briefly, AuNPs were synthesized by either the Turkevich method[22,23] or the Stucky method.[24] All glassware was scrupulously cleaned by immersion for 24 h in a base bath of saturated sodium hydroxide in isopropanol, triple rinsed with distilled water, rinsed with freshly prepared aqua regia and triple rinsed again with distilled water. For the Turkevich method, 13.3 ml of 29 mmol l^{-1} $HAuCl_4$ was added to 1.6 l boiling distilled water, followed by addition of 60 ml of 34 mmol l^{-1} trisodium citrate, then 5 ml of 10 mmol l^{-1} $NaBH_4$ drop-wise. For the Stucky method, 10 µl of dodecanethiol was added per 1 ml of a 40 mmol l^{-1} $AuPPh_3Cl$ toluene solution, followed by addition of an equal volume of 115 mmol l^{-1} *t*-butylamine borane. The Stucky method was typically performed on the 10 ml final volume reaction scale and resulted in typically 78 mg of nominally 6 nm AuNPs. For either method, after 24 h the AuNPs were washed by centrifugation once and the pellets were resuspended in a volume of fresh solvent equal to the original amount. MPS was then added to a solution of AuNPs under vigorous stirring in a prescribed stoichiometric ratio to the AuNP surface area (discussed below). This created the ligand shell. After reaction for 1 h, another wash by centrifugation was performed, with pellets resuspended in distilled water regardless of original solvent. Again based on prescribed stoichiometry, on the order of a few microliters of tertiary amine or quaternary ammonium were added to a 50 ml batch of MPS-coated AuNPs to create the canopy. After reaction for 4 h, the Au NPL was again washed by centrifugation. Note that the quaternary ammonium is reacted with the ligand via a cationic exchange, whereas the amine is reacted via an acid–base reaction. In the latter, the extent of coupling can be monitored by the change in the solution pH (the acidic ligand shell is neutralized by the basic amine canopy). However, the absolute molecular equivalence between the bound ligand and canopy molecules may be overestimated with regard to the amount of unbound, excess ligand in the system that remains after the initial ligand exchange to form the ligand shell, as well as the magnitude of the equilibrium constant of the acid–base reaction. Also the stability of this ionic couple, especially with regard to cationic impurities in the reaction medium is not guaranteed *a priori*.

† Certain trade names and company products are mentioned in the text or identified in illustrations in order to specify adequately the experimental procedure and equipment used. In no case does such identification imply recommendation or endorsement by National Institute of Standards and Technology, nor does it imply that the products are necessarily the best available for the purpose.

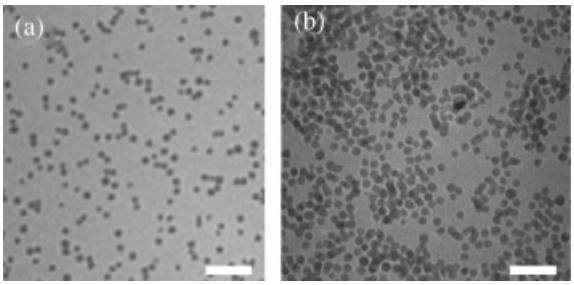

Figure 1. TEM of AuNPs synthesized via the Turkevich method. (a) Crude product (6.2 ± 0.7 nm), (b) after 60% volume reduction of solution by rotary evaporation (6.0 ± 0.7 nm). Scale bars are 50 nm.

To expand, three critical aspects of Au NPL fabrication (evaporative concentration of AuNP solutions, reactant purification by centrifugal washing and determining reactant ratios) are further elucidated below.

Concentrating AuNP solutions

To reduce liquid volume and enable reasonable scale-up of products (increased production mass of NPLs per reaction volume), the initial crude aqueous AuNP products were first concentrated by rotary evaporation prior to surface functionalization. For example, citrate AuNPs were concentrated by rotary evaporation under a stream of N_2 at 80 °C for up to 2 h until approximately 60% of the original volume of solvent (e.g. 1.6 l to 600 ml water) remained. Solutions were monitored visually for flocculation of the AuNPs, and if observed evaporation was halted immediately. If left unchecked, these insoluble aggregates floated to the surface of the solution and significantly decreased recovery yield. Transmission electron microscopy (TEM) of aliquots before and after rotary evaporation revealed that no significant change in size, shape or polydipserity occurred during the rotary evaporation process, as shown in Fig. 1. The relative increase in concentration is also qualitatively observed.

Centrifugal washing of products

Removal of excess reactants was performed by centrifugal washing. In general, centrifugations at 7000 relative centrifugal force (rcf) to 14 000 rcf for 15 min to 90 min were sufficient to pellet AuNPs from the reaction mixtures. Au concentration during the washing was monitored by ultraviolet–visible–near infrared (UV–vis) spectroscopy.

Although benchtop centrifuges enabled more rapid collection of solids for an equivalent rcf, less than 50% of AuNPs were recoverable after one cycle. In contrast, larger capacity centrifuges increased the percent AuNP recovery (up to 71%) due to longer centrifugation times and thus a greater integrated force experienced by the solutions. Despite longer processing times (2 h vs 30 min), the larger capacity enabled an increased throughput (293 mg pure AuNP/day from 6 l stock vs 9.1 mg pure AuNP/day from 288 ml stock). These larger volumes enabled reduction of variability by enabling systematic series of NPLs, such as those with different canopies or changes in concentration of cationic surfactant, to be fabricated from a single stock.

Chemical analysis of samples by inductively coupled plasma atomic emission spectroscopy (ICP-AES) and UV–vis for determination of AuNP concentration was performed on crude AuNPs, washed and resuspended AuNP pellets, and supernatants. As reported in Table 1 for citrate AuNPs, a range of 50–75% of crude Na content was removed after one centrifugation cycle based on ICP analysis of the supernatant. The UV–vis absorption at 520 nm was used to compare the concentration of AuNPs in the solution prior to centrifugation with that of the recovered pellet dispersed in an equivalent volume, and provided the percentage of AuNP recovered during the processing step. After two washings, approximately 30 and 43% of the original AuNPs were retained for small and large centrifugal systems, respectively. Overall, four to five washing cycles were normally possible before the pellets would not resuspend. This was due to the dynamic equilibrium between stabilizing ligands on the surface of the AuNP and those in solution, and thus the requirement of a minimum critical free ligand concentration to stabilize the AuNP solutions existed. When the concentration of free ligand was reduced, desorption of bound ligand occurred to reestablish equilibrium.[25]

Table 1. Yield and degree of purification of citrate AuNP by centrifugation. Values are the means of three experiments, with one standard deviation uncertainty

Volume per batch	Centrifuge time @ 14 000 rcf	Wash 1: percentage AuNP in pellet	Wash 1: percentage Na in supernatant	Wash 2: percentage AuNP in pellet
24 ml	30 min	46 ± 3%	53 ± 8%	66 ± 7%
3.0 l	120 min	71 ± 5%	72 ± 11%	61 ± 5%

Reactant ratios

Complex nanoparticle architectures depend on the synthesis conditions.[26–30] To minimize the amount of unreacted ligand or canopy reactants and their contribution to impurities in the final NPL, reactions were designed with regard to the stoichiometry of the number of surface Au atoms, and not the total number of Au atoms within the AuNP. In the limit of a sphere,[31] the number of surface atoms, N_{surf}, is related to the diameter of the sphere, D_{NP}, as:

$$N_{surf} = N_{NP} - N_{core} = \frac{\pi[{D_{NP}}^3 - (D_{NP} - 2d_{Au})]}{6v_{Au}}, \quad (1)$$

where N_{NP} is the total number of atoms in the spherical volume, N_{core} is the number of atoms not intersecting the surface of the sphere, and d_{Au} and v_{Au} are the diameter and volume of the atom, respectively. The relative fraction of atoms on the AuNP surface, χ_{surf}, then is approximately

$$\chi_{surf} = \frac{N_{surf}}{N_{NP}} = 1 - \frac{(D_{NP} - 2d_{Au})^3}{{D_{NP}}^3}. \quad (2)$$

For example, a 6.0 nm AuNP has 26% of its atoms on the surface (Au: $v_{Au} = 0.0170\ nm^3$, $d_{Au} = 0.288$ nm). Thus, ligand exchange would be based on $\chi_{surf} = 0.26$ multiplied by the total number of Au atoms in the AuNP.

Experimentally, the concentration of surface Au atoms was confirmed from the molar absorptivity of the colloidal solution and microscopic validation of the mean AuNP size. The total number of Au atoms bound into AuNPs was calculated using the molar absorptivity coefficient of each Au atom bound into a AuNP, as described by Mie's calculations.[32,33] For example, each Au

atom bound into a 6.0 nm diameter AuNP has a molar absorptivity coefficient of approximately 3.9×10^3 l mol^{-1} cm^{-1}.[34–36]

Thus, by using Beer–Lambert's law, the concentration of surface Au atoms in a solution of AuNPs (the concentration of Au atoms actively available to participate in a thiol place-exchange reaction) can be approximated from the absorbance

$$C_{\text{surfAu}} = \frac{A}{\varepsilon b \chi_{\text{surf}}} \quad (3)$$

where C_{surfAu} is the estimated concentration of surface Au atoms, A is the measured absorbance, ε is the molar absorptivity coefficient of Au atoms bound into AuNPs, b is the cell pathlength for the measured absorbance, and χ_{surf} is defined in equation (2). The MPS : surface Au ratio on the AuNPs is 1 : 1.8 considering thiol self-assembled monolayers on planar Au[37–39] and recent X-ray crystallography for a 1.49 nm AuNP.[40] The stochiometric concentration of reactants relative to Au should thus be reduced by 1.8 to express the correct equivalence.

Characterization

For TEM experiments, a 4.0 µl drop of the diluted sample was placed on a 400 copper mesh TEM grid with Formvar–carbon support film. The solvent was allowed to evaporate overnight, then images were collected at 200 kV accelerating voltage on a Phillips CM200 LaB6. Images were analyzed using NIH Image J, freely available for download from the internet.[41,42] No less than three images containing no less than 100 particles per image were analyzed to generate sizing statistics. The software scale (pixels/nm) was set from the digitally imprinted scale bar on the TEM images, then the 'Analyze Particles' routine was run with a size range of 50 pixel^2 to infinity pixel$^{[2]}$ and a circularity of 0.50–1.00 a.u. For scanning tunneling microscopy (STM) experiments, an RHK-instruments ultra-high vacuum STM system was used. Solutions of AuNPLs were evaporated onto an atomically smooth Au substrate on a hot plate at 50 °C, and imaged under high vacuum. Zeta-potential measurements were made using a disposable folded electrode on a Malvern Zeta-Sizer Nano system. X-ray photoelectron spectroscopy (XPS) observations were performed on a Surface Sciences Instruments ESCA/XPS; a drop of the diluted sample was placed on a silicon wafer and dried under N_2. Inductively coupled plasma atomic emission spectroscopy (ICP-AES) solutions were diluted to 50 ml before aspiration into a ThermoElectron ICP-AES, with 50 ml of distilled water used to wash the instrument between samples. UV–vis experiments were performed using 1.5 ml polystyrene disposable microcuvettes in a Varian Cary 5000 UV–vis spectrophotometer. The microcentrifuge was an Eppendorf Mini Spin Plus used with the standard rotor and 1.5 or 2.0 ml polypropylene centrifuge tubes. The large centrifuges were a Sorvall Evolution RC centrifuge with an SLA3000 rotor and a Beckman Coulter Alegra X-12. Typically, spin times were increased by a factor of 4 at the same RCF as the microcentrifuge. For electrical observations, Au NPLs which previously had the water solvent evaporated were dropcast onto glass slides, and a probe station was used to bring two conductive probes into contact with the Au NPLs. The distance between the probes was measured, and then the resistance was observed using a Fluke handheld digital multimeter.

RF-MEMS switch performance evaluation was performed on a custom-designed precision instrument which allowed control over contact forces, cycle rates, currents, voltages and position of contact. Details of the engineering and construction of this instrument and specific test conditions employed testing NPL-coated RF-MEMS switches have been published elsewhere.[1,2,11] Briefly, a metal ball provides one electrode that is pushed down into contact with the base electrode. The base electrode was coated with a sub-monolayer of Au NPLs at approximately 10% surface coverage via spin coating.[1,2] The metal ball makes electrical contact with the base electrode to complete the circuit, and is then lifted up to create the open circuit condition.

Results and Discussion

NPL Synthesis and Characterization

The overall fabrication procedure is summarized in Scheme 1. AuNPs are synthesized by one of several well-established methods, such as the Turkevich[22] for 6–30 nm diameter water-soluble AuNPs or the Stucky method for 6 nm diameter organic-soluble AuNPs.[24] After concentration and removal of excess reactants from the initial AuNP synthesis, a ligand exchange reaction is performed with an omega-functional thiol-sulfonate molecule to allow either downstream acid–base chemistry or ion-exchange chemistry to yield a NPL with an organic, ionic corona in the final step of Scheme 1. This is similar to prior reports.[1–3,15–18,22] For example as shown in Fig. 2, AuNPs functionalized with AD can demonstrate liquid-like properties at room temperature on the time scale of minutes after the solvent was evaporated, and AFM

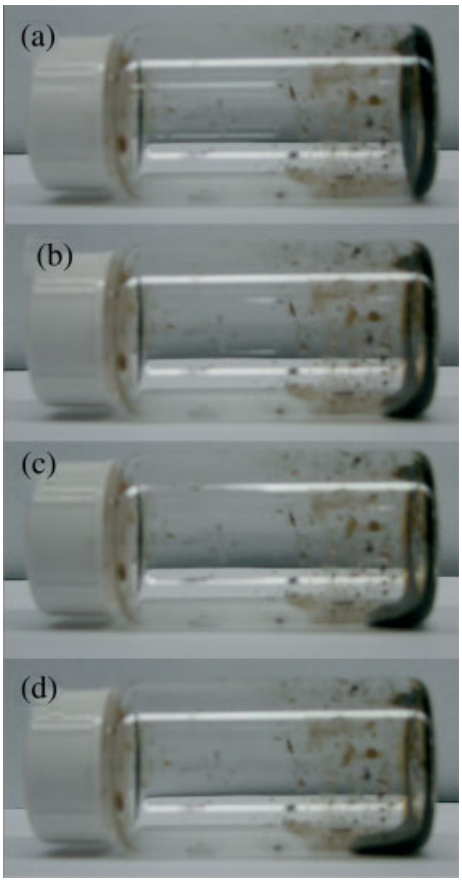

Figure 2. Time-lapsed series of photographs of AD-based nominally 20 nm NPL flowing down the side of a vial at (a) 0 min, (b) 2 min, (c) 5 min, (d) 10 min.

nanolithography experiments have that shown NPL coatings tens of nanometers thick have self-healing properties on a time scale of tens of minutes.[1,2]

Three critical assumptions underlie the generality of this scheme with respect to different initial crude nanoparticle sources and the ability to reliably execute one-pot synthesis. First, the initial ligand exchange reaction is independent of the starting AuNP and associated capping agents. Second, the subsequent formation of the electrostatic couple is quantitative. That is, it is robust to non-bound reactants, does not differentiate between bound and free moieties, and the final product is independent of the canopy coupling approach, i.e. ionic exchange or acid–base reactivity. Third, the products, whether intermediate or final, are purifiable. However, due to the long-range nature of electrostatic interactions and the inherent difficulty in purifying amorphous liquid mixtures short of re-crystallization or evaporation, control of the purity of the intermediate and the final NPL is not *a priori* straightforward. Together, these assumptions and the implications pose numerous challenges to reproducibility and quantification of the chemical and structural aspects of the NPL, including validating the surface density of the moiety that is covalently bound to the AuNP, assessing the extent of removal of un-reacted reagents and estimating the extent of ion-exchange or acid–base coupling at the AuNP surface. These challenges are compounded when limitations to the maximum temperature and reactant concentration are taken into consideration with regard to thermally induced coarsening, thiol-mediated etching,[43–46] and the necessity to keep the AuNPs soluble throughout the synthesis.

Essential to verifying these three critical assumptions is the ability to purify the reaction products. The validation of repeated centrifugal washing to control composition at the three fabrication steps (crude NP, ligand exchange, and canopy assembly) is summarized for the crude NP step in the experimental section (Table 1). Using this approach, the impact of excess reactant concentration on the subsequent reaction step was examined, as well as the role of these molecules on the stability of the AuNP dispersion in the reaction media. Overall, it was found that the type of starting AuNP, either citrate-capped AuNP or dodecanethiol-capped AuNP, did not affect the formation of a NPL. For example, MPS ligand exchange reaction with either AuNP source resulted in MPS–AuNP (same product) as confirmed by XPS and ζ-potiential. Also, for the canopy assembly process, both tertiary amine and quaternary ammonium yielded comparable Au NPLs as verified by similar N content (XPS).

Control of product purity and solution stability enables examination of architectural aspects of the NPL, including control of the surface charge density of the covalently bound anionic ligand-shell and the extent of electrostatic coupling between the organic cation and this surface bound anionic layer. The surface density of the covalently bound ligand-shell establishes the absolute upper limit on the thickness and molecular architecture of a charge-equivalent corona. Clearly, the amount of ionic omega-functional thiol added in the first reaction of Scheme 1 will impact the final surface density of the electrostatically bound canopy. Previous work on nominally 1–2 nm AuNPs suggested that stoichiometry between 150–500 times molar excess thiol ligands was necessary.[43,44] Here, lower ligand concentrations were explored to reduce downstream purification demands.

The average ζ-potential for the 30 nm citrate AuNPs in water with an absorbance of 1.0 was observed to be -58.4 ± 1.9 mV. Figure 3 summarizes how the ζ-potential increased to -37.5 ± 4.8 mV with increased concentration of MPS. Note that the

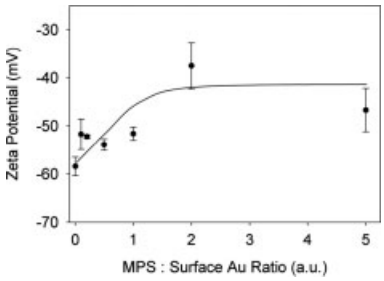

Figure 3. Zeta-potential measurements on purified intermediate products, here 30 nm MPS–AuNPs. The plot of mean ζ-potential as a function of MPS : surface Au reaction stoichiometry contains a line drawn to guide the eye towards the trend.

ζ-potential measurements are after 4 h of mixing, followed by one washing by centrifugation to remove displaced citrate and any excess MPS molecules. Figure 3 shows the mean ζ-potential as a function of ligand : Au surface atom ratio. The symbols in this plot represent the mean and one standard deviation of five observations. At small concentrations of MPS, the ζ-potential increase was very small in magnitude, shifting from -58 ± 2 to -53 ± 3 mV. As an excess of MPS is achieved, the ζ-potential decrease is much greater, changing to -38 ± 5 mV at the 2 : 1 ratios of MPS : surface Au atoms. Recall that a fully dense ligand shell is approximately 1 MPS:1.8 surface Au atoms, thus there was an approximate 4-fold excess of MPS in the final ζ-potential reaction conditions, consistent with the necessity to conduct the exchange using excess reactant.

XPS and Fourier transform infrared (FTIR) spectroscopy of dried assemblies of these purified AuNPs confirmed the increasing extent of exchange. The disappearance of peaks between 2500 and 3000 cm^{-1} in the FTIR spectra (see the Supporting Information) suggests displacement of citrate from the surface of the AuNPs. The corresponding increased presence of MPS on the surface of the AuNPs was reflected by the appearance of S peaks in the XPS spectra. The sulfur content saturated at the reactant ratio of 2 MPS : 1 surface Au atom. Also, the purified MPS–AuNP intermediate was found to be free of Na atoms in all of the XPS spectra collected, implying the sulfonate group is protonated due to the acidic citrate present in the reaction. Note that analysis of the crude product by XPS showed a sulfur content that continually increasing with reactant ratio due to the presence of both bound and free MPS. Also, the crude product contained Na, which reflected the excess citrate molecules. By using the ratio of peak intensities and the inelastic mean free path (IMFP) of electrons (see Supporting Information for details), XPS data suggested 52% of the surface Au atoms reacted with MPS molecules at saturation. This 1 : 2 ratio of the S : Au surface atom is close to the anticipated theoretical estimate of 1 : 1.8 or reaction with 56% of the AuNP's surface Au atoms.[40] Thus, the yield of MPS : thiol binding sites was 93%.

While the use of an excess of thiol will drive the ligand exchange reaction, the extreme excess reported in the literature was not necessary. The combination of centrifugal purification and ζ-potential provided a facile indicator of the ideal reactant ratio. Without purification, the excess thiol compromised the ability to assess the canopy assembly vs the creation of electrostatic couples with un-reacted, but un-removed, thiol reagents. For example, unreacted ligand would positively bias the total quantity of canopy molecules to include both unbound ion pairs mixed with surface bound ion pairs. The difference between bound and

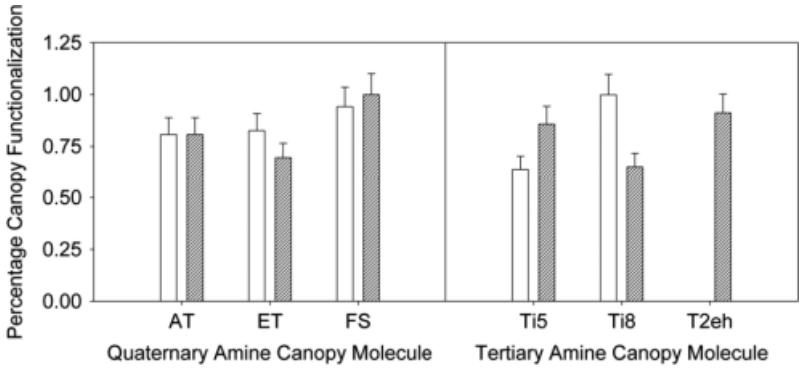

Figure 4. Percentage of canopy functionalization (derived from XPS) of nominally 12 nm AuNPs with ammonium molecules Arquad T-50 (AT), Ethoquad T/13-27 W (ET), MaSurf FS-1620 (FS), triisopentylamine (TI5), triisooctylamine (TI8) and tris(2-ethylhexyl)amine (T2EH). White bars and shaded bars represent a canopy : ligand reaction stoichiometry of 10 : 1 and 1 : 1, respectively.

unbound pairs could not be distinguished by reaction monitoring based on titration. For the AuNPLs discussed below the ligand shell was created from the lowest MPS reactant: surface Au atom stoichiometry yielding saturation, 2 : 1.

The ideal NPL contains an electrostatic equivalence between ligand and canopy within the corona and no unbound ionic pairs. Both an acid–base (alkyl amine) and an ionic exchange (alkyl ammonium chloride) reaction should result in the same product. To probe whether these different approaches for canopy attachment could succeed, a series of NPLs were synthesized from the same intermediate MPS AuNP product batch, which was fractioned off to react with different canopy molecules. Characterization by XPS relied upon the appearance of the N peak from the ammoniums for quantitative confirmation of the reaction. The same technique described in the previous section to determine reaction yields, using the IMFP and ratios of N, S and Au peak intensities against predicted stoichiometries for 100% monolayer formation, was used to collect data such as in Figure 4. The uncertainty bars represent one standard deviation of the mean percentage yield of canopy attachment based on three separate experiments. The vast majority of excess reactant was removed after the first washing step. Subsequent washings did not drastically alter the chemical composition; however irreversible aggregation began to occur after three to four washings. As with the MPS exchange step, this was probably driven by the dynamic equilibrium between the cationic canopy molecules and unbound electrolytes in the solution.

Qualitatively, Fig. 4 shows that the same basic products could be achieved using either ionic exchange with quaternary ammonium (AT, ET, FS) or acid–base chemistry with tertiary amines (TI5, TI8, T2EH). FTIR spectra confirmed the reaction of the canopies with the MPS–AuNPs to form a cationic ammonium (see the Supporting Information). Also, the use of a 10 : 1 molar excess of canopy reactant to ligand molecules (white bars) usually did not, outside of TI8, substantially increase the equivalence within the corona compared with a 1 : 1 molar ratio (shaded bars) of canopy to ligand. The 10 : 1 ratio of T2EH was not observed. As was the case with the MPS ligand exchange reaction onto the AuNPs, similar results were observed whether the starting AuNP was synthesized by the Stucky or Turkevich method.

Typically, between 50 and 85% of the MPS were associated with an ammonium cation after washing. Presumably the remaining sulfonate groups were still acidic, as Na was absent in the XPS spectra. This observation was attributed to crowding at the nanoparticle surface, where the area per anion of the covalently bound ligand shell was substantially smaller than the effective cross-sectional area of the bulky organic ammonium cation. For example, for trioctylamine and MPS, based on the ratio of cross-sectional area of the van der Waals (vdW) volume of each molecule, only 63% of the MPS could minimize the distance between ions due to steric restraint. This created a distance-dependent binding strength between the sulfonate and ammonium, such that not all ion pairs were equally bound. Subsequently, this resulted in either an incomplete initial exchange (i.e. not all the initial sulfonate groups are reacted) or partial removal of the cationic ammonium during the washing due to the dynamic equilibrium that exists between free and surface bound electrolytes. The apparent weak stability of these electrostatic couples contrasted with that observed for layer-by-layer polyelectrolyte assembly. In that case, the stability is ascribed to the poly-ionic nature of the cation and anion, which necessitates simultaneous decoupling of the ion pairs across the entire polymer for desorbtion of the chain, rather than only a single thermally activated desorption event for the NPL. Thus, an ideal NPL corona consisting of single composition with electrostatic equivalence necessitates controlled spacing of the charges within the ligand shell and/or a polyionic (e.g. di or tri) molecular canopy. Note that the mixture of small (H^+) and large cations within the current NPL corona should impact intra- and inter-canopy dynamics. The protons will provide an effective defect density, providing a enhanced mechanism for facile exchange between anion sites and increase fluidity of the canopy.

Fig. 5(a, b) shows AuNPs synthesized with a stoichiometrically matched amount of surfactant ligand, here AD, to available binding sites. The arrows in the Fig. 5(b) indicate the minimal amount of remaining organic material between AuNPs. Fig. 5(c, d) shows two unpurified samples, containing two times and four times excess canopy molecules, respectively, compared with the number of available ligand binding sites. The arrows point to the larger amounts of remaining excess organic material between the AuNPs. As many amines and ammoniums are liquids at room temperature, unpurified products synthesized with great excesses of canopy amine resulted in a suspension of AuNPs in the liquid amine. However, with rigorous purification and characterization of NPL materials before fundamental study of the chemical structural–physical property relationships, this situation can easily be avoided. Figure 6 shows optical images of typical AuNPL black- and gold-colored waxy solids, in this case corresponding to purified TI8 and T5 NPLs from nominally 20 nm AuNPs, respectively.

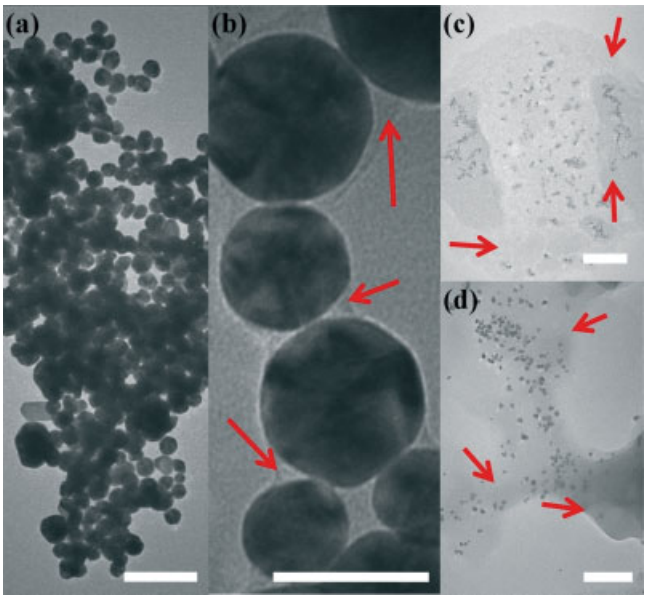

Figure 5. TEM micrographs of AD NPL products from nominally 20 nm AuNPs with different levels of purity. (a) purified, stoichiometrically matched canopy : ligand NPL product with (b) higher magnification image of minimal amounts of organic material between AuNPs; (c) unpurified NPL with 2X molar excess canopy; and (d) unpurified NPL with 4× molar excess canopy. Red arrows point to remaining organic material between AuNPs. Scale bars are 200 nm in a, c, and d; 20 nm in b.

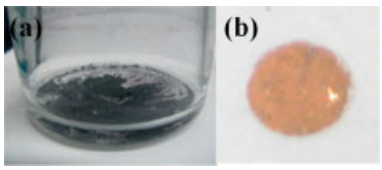

Figure 6. Optical images of example purified NPL products from nominally 12 nm AuNPs. On the left is (a) triisooctylamine canopy, and on the right is (b) tripentylamine canopy.

Another method of visualizing the degree of reaction completion on the AuNP surfaces is to image the molecules on the AuNP surface by STM. Figure 7 shows a three-dimensional representation of the topography by STM of a single AuNP made from SL15 and MPS functionalization of an initially nominally 20 nm citrate AuNP. This canopy molecule was selected due to its high molecular weight and long unsaturated aliphatic chain, with the intention of facilitating STM imaging. As the corona thickness is only 2–3 nm,[47] tunneling current is still able to pass from the STM tip through the AuNP to the substrate.

In general, the STM image shows that the NPL has a significant organic corona surrounding the AuNP. The image is significantly different from that observed for bare Au or Au NPs,[48,49] and more similar to alkane thiol modified Au NPs, for example shown by Stellacci and coworkers.[50] The individual pillars on the surface of the hemisphere are individual molecules of the SL15 quaternary ammonium surfactant, suggesting the reaction was completed successfully. It was possible that the pillars were all oriented normal to the surface of the substrate due to the electric field created by imaging with the STM tip, as in the absence of this aligning field the molecules would be expected to be randomly oriented with respect to the surface of the AuNP. Considering that the area of each pillar (nominally 1.4 nm^2) was approximately the

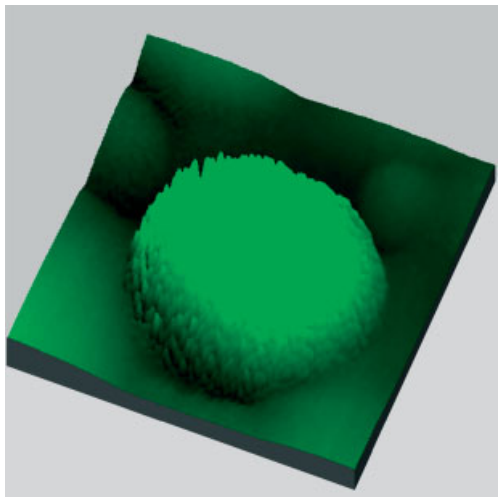

Figure 7. Three-dimensional representation of an STM image of a purified AuNPL made from nominally 20 nm diameter AuNPs. Individual pillars represent each cylindrical corona molecule SL15. Image scale: each side of the square of the surface is 30.0 nm long, while the height scale is 40 nm.

area of an SL15 (nominally 1.1 nm^2) canopy molecule, the STM image provides a direct measurement of the number of molecules present on the surface of the AuNP. The corona's areal density was similar to the N content per AuNP determined from the XPS N : Au ratio.

While no single characterization technique was completely convincing by itself, when a combination of techniques (STM, XPS, FTIR, and previously published SANS[47]) was considered, the data all strongly suggested that that excess reagents including unbound ligands were successfully removed via centrifugal washing and that purified NPLs received a corona with a sub-stochiometric ligand-canopy couple. Equivalence was challenged due to the incommensurate areal charge density of the ligand shell and the proportional immensity of the organic cationic molecules that comprised the canopy.

Corona–Conductivity Relationships

Electron transport through an AuNP assembly will depend exponentially on the distance between AuNPs in accord with variable range hopping or tunneling probability.[51] For a close-packed NP arrangement, the mean distance between particles is related to the cube root of the volume fraction of corona. The size of the NPL corona is a function of the chemical structure of the corona, including molecular weight or degree of branching, which provides increased volume and therefore distance between NP. However, the chemical structure of the canopy also affects the extent of canopy exchange and therefore ultimately the final organic fraction. Thus, the conductivity of NPLs should be highly sensitive to the extent of purification as well as the structure of the corona, and in particular the molecular structure of the canopy.

In contrast to NPLs, electrical transport between AuNPs has been extensively studied.[52–54] For larger diameter AuNPs and higher temperatures, particle-to-particle processes, such as tunneling or hopping, determine the macroscopic conductivity. For smaller AuNPs with diameters of 1–2 nm, Coulomb blockage becomes observable at room temperatures.[55] The field of molecular electronics suggests chemistry can be used to tailor physical properties such as electrical properties.[56,57] Thus, to

Table 2. Structure–property relationship between NPL corona chemistry and NPL bulk resistance

Molecule	MW (*u*)	Branching	N : S ratio	Organic volume fraction	Bulk AuNPL R/d (Ω/cm)
Trioctyl amine (T8)	353	None	0.74	0.23	1.56×10^8
Trihexyl amine (T6)	269	None	0.69	0.17	5.07×10^5
Tripentyl amine (T5)	227	None	0.65	0.14	6.95×10^2
Triisopentyl amine (TI5)	227	Distal	0.61	0.14	4.50×10^2

R/d: resistance per unit distance

maximize macroscopic conductivity of the assembly, the distance between AuNPs must be minimized, either via post-deposition thermal treatments to encourage nanoparticle coalescence or by minimizing the volume fraction of the insulative organic corona.[30,58–64] The latter approach was used in this study, as it was important to avoid particle coalescence for the particle surface mobility required for surface self-healing of the electrical contact mentioned in the introduction and further described below.

Conductivity measurements were performed on purified bulk NPL samples after the solvent was evaporated. Table 2 summarizes the molecular weight, type of branching in the canopy molecular structure, extent of canopy exchange, organic volume fraction and the resistance measured per unit distance for four purified NPLs with a nominally 20 nm diameter AuNP core. The fraction of MPS ligands that reacted with amine canopy molecules was observed by the XPS atomic composition ratio of N : S, and considering the stoichiometry of the ligand and canopy molecular formulae. Overall the resistance spans several orders of magnitude and in general scales with organic volume fraction. For example, the first three rows of Table 2 show three NPLs with coronas of decreasing molecular weight (T8, T6, T5). A decreasing bulk resistance measurement was observed as the organic volume fraction of the NPL decreased, although approximately 70% of canopy molecules exchanged into the corona. Further agreement with this qualitative trend was observed when two molecular architectures of the same molecular weight (T5 and TI5) were used as canopy ligands and produced bulk NPLs with similar resistance measurements.

Figure 8 summarizes a broad collection of Au NPLs resistivities, both purified and containing excess canopy molecules, across the entire range of core AuNP diameters included in this study, where points are the mean of no less than three measurements with uncertainty of one standard deviation. A detailed table containing the specific canopy molecule and degree of purification is provided in the Supporting Information. For the RF-MEMS device switch discussed below, resistance values of AuNPLs lower than 10^6 ohm cm^{-1} are desirable. In general, the resistivities scale exponentially with the volume fraction of organic, although sufficient scatter in the results confound more detailed analysis, such as comparison with hopping models where the resistivities would depend on the cube root of the organic fraction, i.e. particle separation. Also, molecular architecture may play a role that is not yet fully understood, an area of future work beyond the scope of this report.

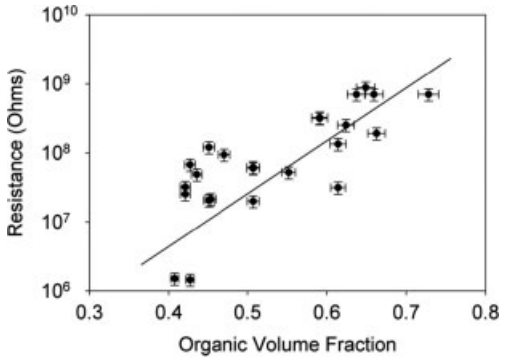

Figure 8. Relation between bulk resistance and organic volume fraction of Au NPLs. Organic volume fraction can be affected by the degree of purity, as well as the canopy molecule selection, thus a detailed table used to construct this figure is provided in the supporting information. Each point represents one measurement, with the vertical uncertainty bars representing the instrumental uncertainty from the resistance measurements and horizontal uncertainty bars representing the uncertainty from chemical composition analysis, performed by ICP-AAS and/or XPS. A line is drawn to guide the eye towards the trend.

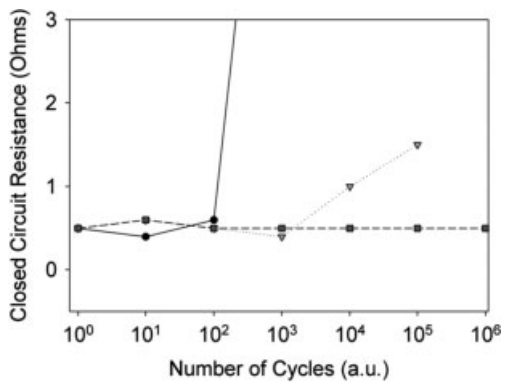

Figure 9. Resistance across closed switch simulator for increasing number of switching cycles at 1 mA current. Circles represent bare Au electrodes, triangles represent Au electrodes coated with crude NPL product (AD canopy, nominally 20 nm AuNP[2]) and squares represent Au electrodes coated with purified AD Au NPL product. Resistance greater than 1 Ω across a closed switch is defined as device failure.

Application to Rf-Mems Switches

RF-MEMS devices have seen increased demand with the proliferation of cell phones and other wireless communication devices. One of the most common architectures engineered in these devices is a relay switch, where physical contact or separation between two electrodes determines the closed or open state of the circuit.[1,12] In order to achieve the fullest potential, these relay switches must perform for 10^9 cycles or greater over their lifetime.[11] Because of the increasingly smooth surfaces used in these relay switches as device scales become smaller, adhesive forces can become so great that the electrodes become irreversibly bound.[65,66] At large current density, local melting of the metal due to Joule heating can lead to thin wires being drawn across the gap as the electrodes withdraw, shorting the open circuit position.

Figure 9 compares the durability improvements under high current conditions (1 mA) for purified NPLs with their crude (unpurified) NPL counterpart that was previously reported.[2] The control bare Au electrode failed on the order of magnitude of hundreds of cycles. Device failure was defined as resistance

greater than one ohm when the switch was in the closed position or a short-circuit condition developed.[11] A sub-monolayer of the crude NPL material, made here from an AD canopy and nominally 20 nm AuNPs, increased device lifetime to the order of 10^4 cycles. However, use of the purified NPL, which had excess organic removed, led to the device performing acceptably for the duration of the test with no signs of degradation in performance. Experiments were halted at 10^6 cycles due to time constraints associated with a maximum cycle rate of 5 Hz. As reported from alkylthiol SAM work,[11] carbon ashing and buildup can occur during high current switching which leads to device failure. While the AD functionalized Au NPL previously exhibited the ability to flow in new nanoparticles to the areas where nanoparticles melted or carbon ash built up,[2] minimizing the organic volume fraction would restrict the amount of carbon ash that could form, enabling more nanoparticles and thus more metal to flow in to the region of switch contact. The NPL materials which exhibited waxy-solid characteristics at room temperature were not studied in the RF-MEMS switch simulator, as evaluating the specific role of a NPL's flowability in device performace was beyond the scope of this report. Nevertheless, this experiment demonstrated the potential increase in device performance for applications that can be realized through the careful control over purification and rigorous characterization achieved in the synthetic scheme proposed in this work, beyond the increased fundamental scientific understanding of NPL materials.

Conclusion

A systematic method of synthesizing larger inorganic volume fraction NPLs has been developed using AuNPs as the model core NP. By focusing on reactant ratios and quantification of chemical content and fate during washing steps, a high degree of control over the purity of the sample was maintained while allowing for easy scalability in batch sizes and synthesis throughput. This synthesis scheme also enabled a single ligand-functionalized core to serve as the base to attach a wide variety of organic canopies via acid-base or exchange reactions. The thorough purification and characterization at each processing step enabled improved reproducibility and chemical analysis of final bulk NPL products. Stable NPLs after purification exhibited a sub-equivalence of canopy-to-ligand ratio. This most likely arose from the incommensurate areal density of anionic charge within the ligand shell relative to the larger size of the cationic canopy molecule. The resultant distribution in cation–anion distance within the corona would manifest in a distribution in the binding energy of the cation–anion pairs, resulting in a population that was more weakly bound, or not originally exchanged in the initial assembly of the canopy and subsequently removed through purification.

Increasing the volume fraction or molecular weight of the corona was found to increase exponentially the resistance of the bulk NPLs, although sufficient variance in the results indicates that numerous mechanisms may be contributing to the final resistivity, thus necessitating detailed future studies such as temperature-impedance spectroscopy. Nevertheless, the increased conductivity and reduced organic fractions arising from the purification methodologies enabled the extension of the working lifetime of RF-MEMS relay switches by at least two orders of magnitude over prior reports.

In conclusion, the high purity and rigorous physical and chemical characterization discussed herein enables greater confidence in chemical structural–physical property correlations for NPLs, which will enable a broader fundamental understanding of this emerging class of materials and better engineering of NPL materials for specific device applications.

Supporting information

Supporting information may be found in the online version of this article.

Acknowledgments

The authors are grateful to the Air Force Office of Scientific Research and Air Force Research Laboratory Materials and Manufacturing Directorate for financial support and to Professor Liming Dai (University of Dayton) for help with experiments.

References

[1] S. T. Patton, A. A. Voevodin, R. A. Vaia, M. Pender, S. J. Diamanti, B. Phillips, *J. Microelectromech. Systems* **2008**, *17*(3), 741.
[2] A. A. Voevodin, R. A. Vaia, S. T. Patton, S. Diamanti, M. Pender, M. Yoonessi, J. Brubaker, J. J. Hu, J. H. Sanders, B. S. Phillips, R. I. MacCuspie, *Small* **2007**, *3*(11), 1957.
[3] E. P. Giannelis, A. Bourlinos, R. Herrera, R. Rodriguez, L. A. Archer, G. A. Floudas, G. Fytas, *Abstracts of Papers of the American Chemical Society* **2006**, *231*.
[4] A. B. Bourlinos, S. R. Chowdhury, R. Herrera, D. D. Jiang, Q. Zhang, L. A. Archer, E. P. Giannelis, *Adv. Functional Mater.* **2005**, *15*(8), 1285.
[5] C. M. Brick, E. R. Chan, S. C. Glotzer, J. C. Marchal, D. C. Martin, R. M. Laine, *Adv. Mater.* **2007**, *19*(1), 82.
[6] M. G. Ancona, S. E. Kooi, W. Kruppa, A. W. Snow, E. E. Foos, L. J. Whitman, D. Park, L. Shirey, *Nano Lett.* **2003**, *3*(2), 135.
[7] F. Carpi, D. De Rossi, *Mater. Sci. Eng. C Biomimet. Supramol. Systems* **2004**, *24*(4), 555.
[8] J. Mackerle, *Modell. Simul. Mater. Sci. and Eng.* **2004**, *12*(5), 1031.
[9] S. S. Ray, M. Biswas, *Synthet. Metals* **2000**, *108*(3), 231.
[10] Guo-Hua Chen, Da-Jun Wu, Wen-Gui Weng, Bin He, Yan P Wen-li, *Polym. Int.* **2001**, *50*(9), 980.
[11] S. T. Patton, K. C. Eapen, J. S. Zabinski, J. H. Sanders, A. A. Voevodin, *J. Appl. Phys.* **2007**, *102*(2), 024903.
[12] S. T. Patton, J. M. Slocik, A. Campbell, J. J. Hu, R. R. Naik, A. A. Voevodin, *Nanotechnology* **2008**, *19*(40), 405705.
[13] U. Landman, W. D. Luedtke, *Faraday Discuss.* **2004**, *125*, 1.
[14] N. Sandhyarani, T. Pradeep, J. Chakrabarti, M. Yousuf, H. K. Sahu, *Phys. Rev. B* **2000**, *62*(2), R739.
[15] S. C. Warren, F. J. DiSalvo, U. Wiesner, *Nat. Mater.* **2007**, *6*(2), 156.
[16] A. B. Bourlinos, R. Herrera, N. Chalkias, D. D. Jiang, Q. Zhang, L. A. Archer, E. P. Giannelis, *Adv. Mater.* **2005**, *17*(2), 234.
[17] A. B. Bourlinos, E. P. Giannelis, Q. Zhang, L. A. Archer, G. Floudas, G. Fytas, *Eur. Phys. J.* **2006**, *20*(1), 109.
[18] A. B. Bourlinos, A. Stassinopoulos, D. Anglos, R. Herrera, S. H. Anastasiadis, D. Petridis, E. P. Giannelis, *Small* **2006**, *2*(4), 513.
[19] A. B. Bourlinos, S. R. Chowdhury, D. D. Jiang, Q. Zhang, *J. Mater. Sci.* **2005**, *40*(18), 5095.
[20] A. B. Bourlinos, S. R. Chowdhury, D. D. Jiang, Y. U. An, Q. Zhang, L. A. Archer, E. R. Giannelis, *Small* **2005**, *1*(1), 80.
[21] R. Rodriguez, R. Herrera, L. A. Archer, E. P. Giannelis, *Adv. Mater.* **2008**, *20*(22), 4353.
[22] J. Turkevich, P. C. Stevenson, J. Hillier, *Discuss. Faraday Soc.* **1951**, (11), 55.
[23] J. Turkevich, P. C. Stevenson, J. Hillier, *J. Phys. Chem.* **1953**, *57*(7), 670.
[24] N. Zheng, J. Fan, G. D. Stucky, *J. Am. Chem. Soc.* **2006**, *128*(20), 6550.
[25] Y. Song, R. W. Murray, *J. Am. Chem. Soc.* **2002**, *124*(24), 7096.
[26] I. A. Banerjee, L. T. Yu, R. I. MacCuspie, H. Matsui, *Nano Lett.* **2004**, *4*(12), 2437.

[27] X. Y. Gao, L. T. Yu, R. I. MacCuspie, H. Matsui, *Adv. Mater.* **2005**, *17*(4), 426.
[28] H. Matsui, R. MacCuspie, *Nano Lett.* **2001**, *1*(12), 671.
[29] N. Nuraje, I. A. Banerjee, R. I. MacCuspie, L. T. Yu, H. Matsui, *J. Am. Chem. Soc.* **2004**, *126*(26), 8088.
[30] N. Nuraje, K. Su, J. Samson, A. Haboosheh, R. I. MacCuspie, H. Matsui, *Supramol. Chem.* **2006**, *18*(5), 429.
[31] D. V. Leff, P. C. Ohara, J. R. Heath, W. M. Gelbart, *J. Phys. Chem.* **1995**, *99*(18), 7036.
[32] J. Duan, K. Park, R. I. MacCuspie, R. A. Vaia, R. O. Pachter, *J. Phys. Chem. C* **2009**, *113*(35), 15524.
[33] S. Link, M. A. El-Sayed, *J. Phys. Chem. B* **1999**, *103*(40), 8410.
[34] X. O. Liu, M. Atwater, J. H. Wang, Q. Huo, *Colloids Surf. B Biointerfaces* **2007**, *58*(1), 3.
[35] G. Mie, *Ann. Phys.* **1908**, *25*(3), 377.
[36] P. N. Njoki, I. I. S. Lim, D. Mott, H. Y. Park, B. Khan, S. Mishra, R. Sujakumar, J. Luo, C. J. Zhong, *J. Phys. Chem. C* **2007**, *111*(40), 14664.
[37] P. K. Ghorai, S. C. Glotzer, *J. Phys. Chem. C* **2007**, *111*(43), 15857.
[38] F. W. Delrio, C. Jaye, D. A. Fischer, R. F. Cook, *Appl. Phys. Lett.* **2009**, *94*(13), 131909.
[39] D. I. Kim, N. Pradeep, F. W. Delrio, R. F. Cook, *Appl. Phys. Lett.* **2008**, *93*(20), 161719.
[40] P. D. Jadzinsky, G. Calero, C. J. Ackerson, D. A. Bushnell, R. D. S. Kornberg, *Science* **2007**, *318*(5849), 430.
[41] M. D. Abramoff, P. J. Magelhaes, S. J. Ram, *Biophot. Int.* **2004**, *11*(7), 36.
[42] *ImageJ*, version 1.40g; US National Institutes of Health: Bethesda, MD, **1997**.
[43] G. H. Woehrle, J. E. Hutchison, *Inorg. Chem.* **2005**, *44*(18), 6149.
[44] G. H. Woehrle, L. O. Brown, J. E. Hutchison, *J. Am. Chem. Soc.* **2005**, *127*(7), 2172.
[45] S. Y. Lin, Y. T. Tsai, C. C. Chen, C. M. Lin, C. H. Chen, *J. Phys. Chem. B* **2004**, *108*(7), 2134.
[46] A. C. Templeton, M. J. Hostetler, E. K. Warmoth, S. W. Chen, C. M. Hartshorn, V. M. Krishnamurthy, M. D. E. Forbes, R. W. Murray, *J. Am. Chem. Soc.* **1998**, *120*(19), 4845.
[47] M. Yoonessi, E. Seikel, M. J. Pender, *Langmuir* **2009**, *25*(6), 3369.
[48] M. Nakai, Y. Yamanoi, Y. Nishimori, T. Yonezawa, H. Nishihara, *Angew. Chem. Int. Edn* **2008**, *47*(35), 6699.
[49] S. Wakamatsu, J. i. Nakada, S. Fujii, U. Akiba, M. Fujihira, *Ultramicroscopy* **2005**, *105*(1–4), 26.
[50] A. M. Jackson, J. W. Myerson, F. S. Stellacci, *Nat. Mater.* **2004**, *3*(5), 330.
[51] N. A. Kotov, *Nanoparticle Assemblies and Superstructures*, CRC/Taylor & Francis: Boca Raton, FL, **2006**.
[52] D. M. Adams, L. Brus, C. E. D. Chidsey, S. Creager, C. Creutz, C. R. Kagan, P. V. Kamat, M. Lieberman, S. Lindsay, R. A. Marcus, R. M. Metzger, M. E. Michel-Beyerle, J. R. Miller, M. D. Newton, D. R. Rolison, O. Sankey, K. K. S. Schanze, J. Yardley, X. Y. Zhu, *J. Phys. Chem. B* **2003**, *107*(28), 6668.
[53] R. K. Smith, S. U. Nanayakkara, G. H. Woehrle, T. P. Pearl, M. M. Blake, J. E. Hutchison, P. S. Weiss, *J. Am. Chem. Soc.* **2006**, *128*(29), 9266.
[54] F. Chen, J. Hihath, Z. F. Huang, X. L. Li, N. J. Tao, *Annu. Rev. Phys. Chem.* **2007**, *58*, 535.
[55] W. Wang, D. Lee, R. W. Murray, *J. Phys. Chem. B* **2006**, *110*(21), 10258.
[56] C. G. Tao, T. J. Stasevich, W. G. Cullen, T. L. Einstein, E. D. Williams, *Nano Lett.* **2007**, *7*(6), 1495.
[57] Z. F. Huang, F. Chen, P. A. Bennett, N. J. Tao, *J. Am. Chem. Soc.* **2007**, *129*(43), 13225.
[58] S. Chen, R. S. Ingram, M. K. Hostetler, J. J. Pietron, R. W. Murray, T. G. Schaaff, J. T. Khoury, M. M. Alvarez, R. L. Whetten, *Science* **1998**, *280*(5372), 2098.
[59] S. Chen, R. J. Pei, *J. Am. Chem. Soc.* **2001**, *123*(43), 10607.
[60] J. F. Hicks, D. T. Miles, R. W. Murray, *J. Am. Chem. Soc.* **2002**, *124*(44), 13322.
[61] G. Schmid, U. Simon, *Chem. Commun.* **2005**, (6), 697.
[62] H. Taube, *Science* **1984**, *226*(4678), 1028.
[63] W. P. Wuelfing, S. J. Green, J. J. Pietron, D. E. Cliffel, R. W. Murray, *J. Am. Chem. Soc.* **2000**, *122*(46), 11465.
[64] R. I. MacCuspie, N. Nuraje, S. Y. Lee, A. Runge, H. Matsui, *J. Am. Chem. Soc.* **2008**, *130*(3), 887.
[65] F. W. Delrio, M. L. Dunn, B. L. Boyce, A. D. Corwin, M. P. De Boer, *J. Appl. Phys.* **2006**, *99*(10), 151329.
[66] F. W. DelRio, K. L. Steffens, C. Jaye, D. A. Fischer, R. F. Cook, *Langmuir*, American Society of Mechanical Engineers, Micro-Electro Mechanical Systems Division, (Publications), American Society of Mechanical Engineers, Chicago, IL, **2010**, *26* (3), 1688–1699.